nature energy

ARTICLES

https://doi.org/10.1038/s41560-020-0558-0



# Quantifying the impacts of climate change and extreme climate events on energy systems

A. T. D. Perera[1,2]✉, Vahid M. Nik[3,4,5], Deliang Chen[6], Jean-Louis Scartezzini[1] and Tianzhen Hong[7]

**Climate induced extreme weather events and weather variations will affect both the demand of energy and the resilience of energy supply systems. The specific potential impact of extreme events on energy systems has been difficult to quantify due to the unpredictability of future weather events. Here we develop a stochastic-robust optimization method to consider both low impact variations and extreme events. Applications of the method to 30 cities in Sweden, by considering 13 climate change scenarios, reveal that uncertainties in renewable energy potential and demand can lead to a significant performance gap (up to 34% for grid integration) brought by future climate variations and a drop in power supply reliability (up to 16%) due to extreme weather events. Appropriate quantification of the climate change impacts will ensure robust operation of the energy systems and enable renewable energy penetration above 30% for a majority of the cities.**

According to the Fifth Assessment Report of the Intergovernmental Panel on Climate Change (IPCC)[1], climate change will most likely accelerate, causing increasingly frequent and strong extreme climate events that make humans, as well as built and natural systems, more vulnerable to those events. Failure to address climate change mitigation and adaptation could lead to serious short- and long-term issues[2], including partial or total blackouts due to energy supply disruptions[3]. These consequences could be very costly to cities and urban areas. Currently, 3.5 billion people live in these areas, consuming two-thirds of global primary energy and producing 71% of the directly energy-related global greenhouse gas (GHG) emissions. By 2050, urban areas are expected to hold more than half of the world's population, which will multiply the costs and impacts[4]. Therefore, the urban sector must play an important role in both climate change adaptation and mitigation. Conserving energy and using renewable energy technologies in these areas will be essential to minimize the carbon footprint of the energy infrastructure. Distributed energy systems that support the integration of renewable energy technologies will support the energy transition in the urban context[5] and play a vital role in climate change mitigation and adaptation.

Climate change affects the energy use of urban areas extensively by influencing energy demand, generation, systems and infrastructure[6,7]. Renewable energy generation can be affected in various ways too, depending on the renewable source (for example, wind, hydropower or solar)[8,9] and geographical location[10]. Due to extreme weather events, the impacts of climate change on peak electricity demand will reach well beyond simple changes in net annual demand and become more critical due to their influence on system design and power supply[11,12]. For example, Sweden's existing residential building stock may experience an approximate 30% decrease in 20-year average heating demand during 2081–2100 compared with 1991–2010, while during extreme conditions the hourly heating and cooling demand may be between 50 and 400% more than the 20-year average values[13]. Such extreme conditions make climate change adaptation difficult[6].

Uncertainty in energy demand, renewable energy potential and grid conditions associated with climate change is defined in this study as the climate-induced energy uncertainty (CInU). CInU can lead to low-probability, high-impact (LPHI) events, usually induced by extreme weather events, and/or high-probability, low-impact (HPLI) conditions, such as variations in average energy demand and generation. LPHI events may lead to blackouts, while HPLI conditions will lead to significant degradation of energy system performance (such as an increase in operation costs), which will notably retard the integration of renewable energy technologies, increasing the dependence on fossil fuels and further accelerating climate change and increasing CInU. Understanding the effect of CInU on energy systems is challenging due to the complexity of the climate and energy systems, high stochasticity and multidimensional impacts[14]. To break the vicious cycle of increasing CInU and to support renewable energy integration, it is vital to quantify the impacts of climate change by translating future climate data into energy system relevant data[15] and using them to design climate-resilient energy systems.

Here we develop a methodology to investigate the impacts of climate change on urban energy systems, taking into consideration future variations in climate conditions, including the increasing frequency, duration and intensity of extreme weather events. We then investigate the impacts of CInU on the performance of urban energy systems and attempt to understand the limitations in integrating renewable energy technologies due to CInU by investigating a wide range of scenarios for 30 Swedish cities.

## Modelling future climate variations and extreme weather

The operational strategies of an energy system are determined by hourly changes in demand, renewable energy generation, grid conditions and other factors. Therefore, time-series data over a 1-year

[1]Solar Energy and Building Physics Laboratory (LESO-PB), École Polytechnique Fédérale de Lausanne (EPFL), Lausanne, Switzerland. [2]Urban Energy Systems Laboratory, EMPA, Dübendorf, Switzerland. [3]Division of Building Physics, Department of Building and Environmental Technology, Lund University, Lund, Sweden. [4]Division of Building Technology, Department of Civil and Environmental Engineering, Chalmers University of Technology, Gothenburg, Sweden. [5]Institute for Future Environments, Queensland University of Technology, Garden Point Campus, Brisbane, QLD, Australia. [6]Regional Climate Group, Department of Earth Sciences, University of Gothenburg, Gothenburg, Sweden. [7]Building Technology and Urban Systems Division, Lawrence Berkeley National Laboratory, Berkeley, CA, USA. ✉e-mail: dasun.perera@empa.ch

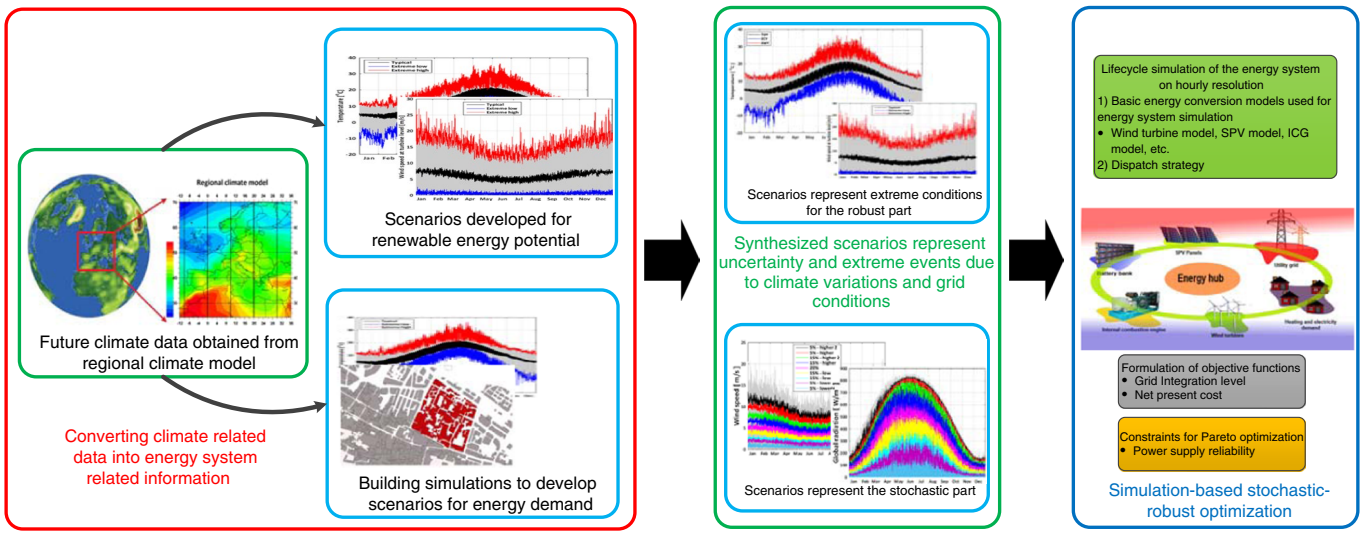


**Fig. 1 | Understanding the influences of future climate changes during energy system design.** The interlinks between the climate model and the energy system model are not straightforward, which makes it difficult to interlink climate models directly with energy system models. As shown in the figure, we develop a workflow to synthesize a pool of scenarios (with the support of an urban simulation model) to link the climate model with the energy system model. SPV, solar photovoltaic; ICG, internal combustion generator.

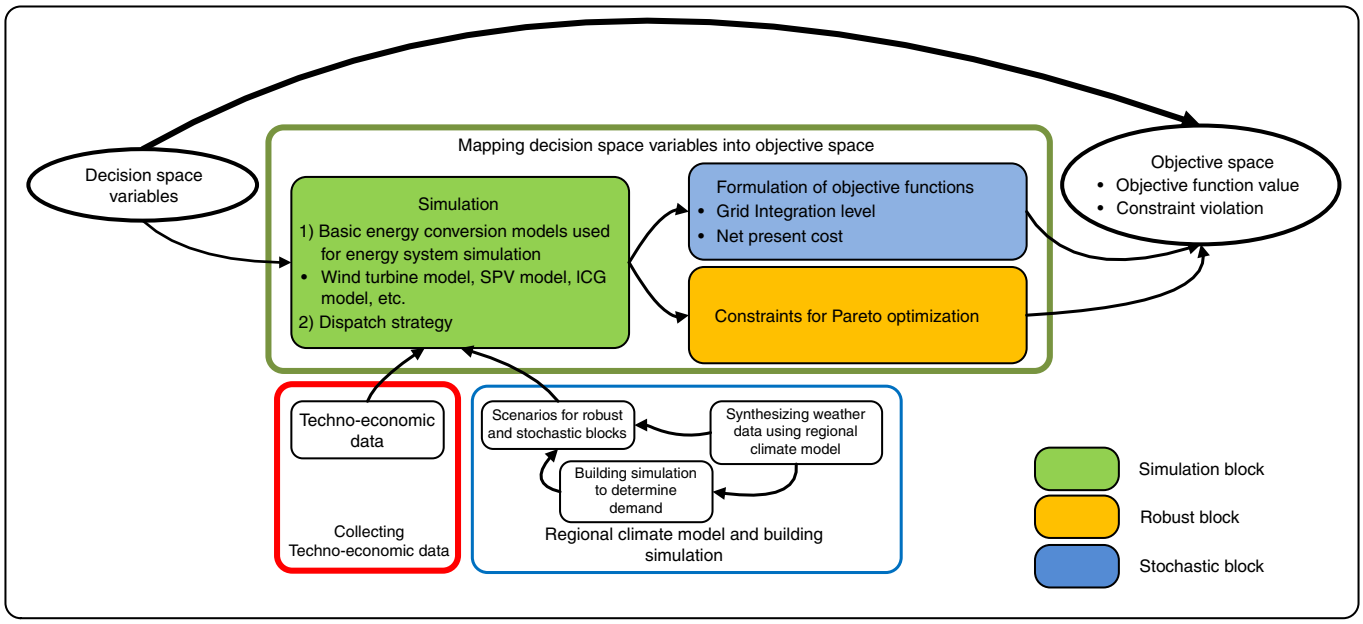


**Fig. 2 | Considering the climate-induced uncertainties in the design phase.** The performance of the energy system is evaluated under HPLI and LPHI scenarios, as explained in the block diagram. The techno-economic and weather data are provided as the input data to the computational algorithm. A common model (Simulation block) is used to present the energy flow for both HPLI and LPHI scenarios. The Stochastic and Robust blocks, respectively, are used to consider the influences of HPLI and LPHI scenarios during the design phase. A comprehensive description of the model is presented in the Methods Section.

period are usually used when designing urban energy systems. This means that although HPLI and LPHI affect both hourly operation strategies and the design of the energy system, they are not being considered in the present state-of-the-art deterministic models. Deterministic models use a single time series to represent demand, renewable energy potential and grid conditions. Therefore, they fail to represent CInU. Even with this limitation, it may take several days to design energy systems considering their hourly operation strategy while using deterministic models[16].

A pool of scenarios is required to consider LPHI and HPLI conditions, and such an evaluation requires a set of time series of energy demand, renewable energy potential and grid conditions. However, the number of scenarios considered needs to be limited, to make the energy system design evaluation process computationally feasible (that is, to avoid the curse of dimensionality issues). Therefore, a set of time series are synthesized (as explained in the Methods section) considering several future climate scenarios as outputs of a regional climate model (RCM) to achieve a better representation of the possible future conditions that the energy system would encounter due to HPLI scenarios (Fig. 1). Each time series within a set is introduced as an 'expected scenario', and the set is defined as a 'set of expected scenarios'. This set of expected scenarios enables users to

obtain a qualitative and quantitative understanding of the changes in weather patterns, and consequently, the expected future conditions (more details can be found in the Methods section).

Similarly, a set of scenarios are introduced to represent the uncertainties in the grid. The set of scenarios obtained to represent HPLI conditions can be used to formulate the stochastic part of the optimization problem (as explained in the Methods section). Subsequently, a robust optimization technique is introduced to guarantee the robust operation of the energy system during extreme weather conditions. Multiple single time series are synthesized to present extreme conditions (LPHI) for demand, renewable energy potential and grid conditions, which constitutes the robust part of the optimization problem. Finally, a hybrid stochastic-robust optimization algorithm is developed (Fig. 2) to consider both HPLI and extreme conditions during the energy system optimization, as detailed in the Methods section.

## Representative energy demand for future climate conditions

The common approach in building and urban energy studies is to use typical weather conditions for simulation purposes[17]. Several types of typical weather data sets, such as typical meteorological year (TMY), are available[18]. In this study we applied typical downscaled year (TDY)[19] for benchmarking. However, climate change may induce more frequent and stronger extreme events, and these can be the events that present the biggest challenge to maintaining an energy system's healthy operation. Extreme cold year (ECY) and extreme warm year (EWY) are defined as the extreme conditions in this study, distinguishing the boundaries at which the system should be capable of operating. Figure 3 illustrates a significant shift in outdoor temperature, energy demand and renewable energy potential when moving from typical to extreme conditions. Seasonal variations are also visible for the extreme conditions, although their patterns can be different from those of typical weather. For example, Fig. 3 shows that energy demand increases due to extreme heating (ECY) and cooling (EWY) demand, respectively, during cold (Jan–Feb and Oct–Dec) and warm (May–Sep) seasons (a detailed description of the methodology used to derive time series for ECY and EWY using RCM weather data is provided in the Methods section). As a result, an energy system designed only for typical conditions may fail to meet the demand during extreme climate conditions, leading to a number of adverse consequences.

Besides extreme conditions, HPLI scenarios (or non-extreme conditions) strongly affect the energy system performance in the long run due to the higher probability of their occurrence compared with extreme conditions. It is difficult to come up with a single time series to present HPLI scenarios for future climate. We have developed four sets of future expected scenarios to present HPLI conditions for the stochastic optimization of the energy system based on (1) energy demand, (2) wind energy potential, (3) solar energy potential and (4) grid conditions (more details are presented in the Methods section). Each set of future expected scenarios consists of three, five, seven and nine scenarios (namely P3, P5, P7 and P9 in Fig. 4a–d) to show the impact that the number of synthesized time series has on representing CInU.

When we analysed the four different sets of scenarios obtained for energy demand, the expected scenarios having the highest probability of occurrence followed the pattern of the typical year (TDY) with moderate energy demand. As a result, seasonal variations such as higher demand in winter and lower demand in summer can be observed. By moving towards the expected scenarios with lower probabilities (moving from the centre to the periphery in Fig. 4), seasonal variations diverge from the typical pattern and converge to patterns more closely aligned with extreme conditions. This is obvious for the sets with a higher number of expected scenarios (for example, in Fig. 4, compare P7-7 with P7-4 and P9-9 with P9-5). Apparently, by increasing the number of synthesized time series, the chances of representing extreme conditions increase. This is elaborated further in Fig. 4e by comparing the distributions of the expected scenarios with extreme scenarios using box plots. Each box displays the interquartile range, which is the range between the 25th and 75th percentiles, and the median is marked by a red line in the box. Whiskers are extended 1.5 times the interquartile range from both sides, and outliers are shown by red dots. According to

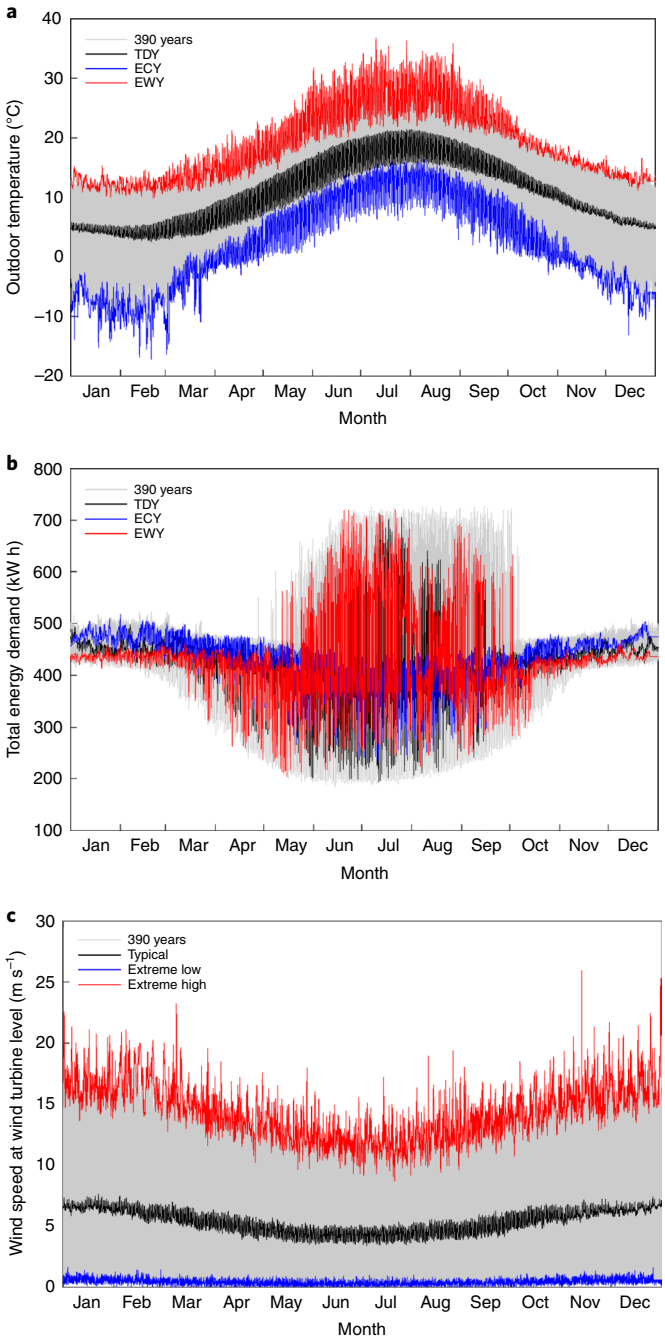


**Fig. 3 | Wind, temperature and energy demand variation under 13 climate scenarios. a–c**, Hourly distributions of the outdoor temperature (**a**), total energy demand (**b**) and wind speed at wind turbine level (60 m, **c**) in Malmö for 13 climate scenarios during 2070–2099 (390 profiles, light-grey lines) and the typical (TDY) and extreme scenarios (ECY and EWY) chosen on the basis of hourly distributions. A significant difference in temperature, energy demand and wind speed can be observed when moving from typical conditions to extremes.

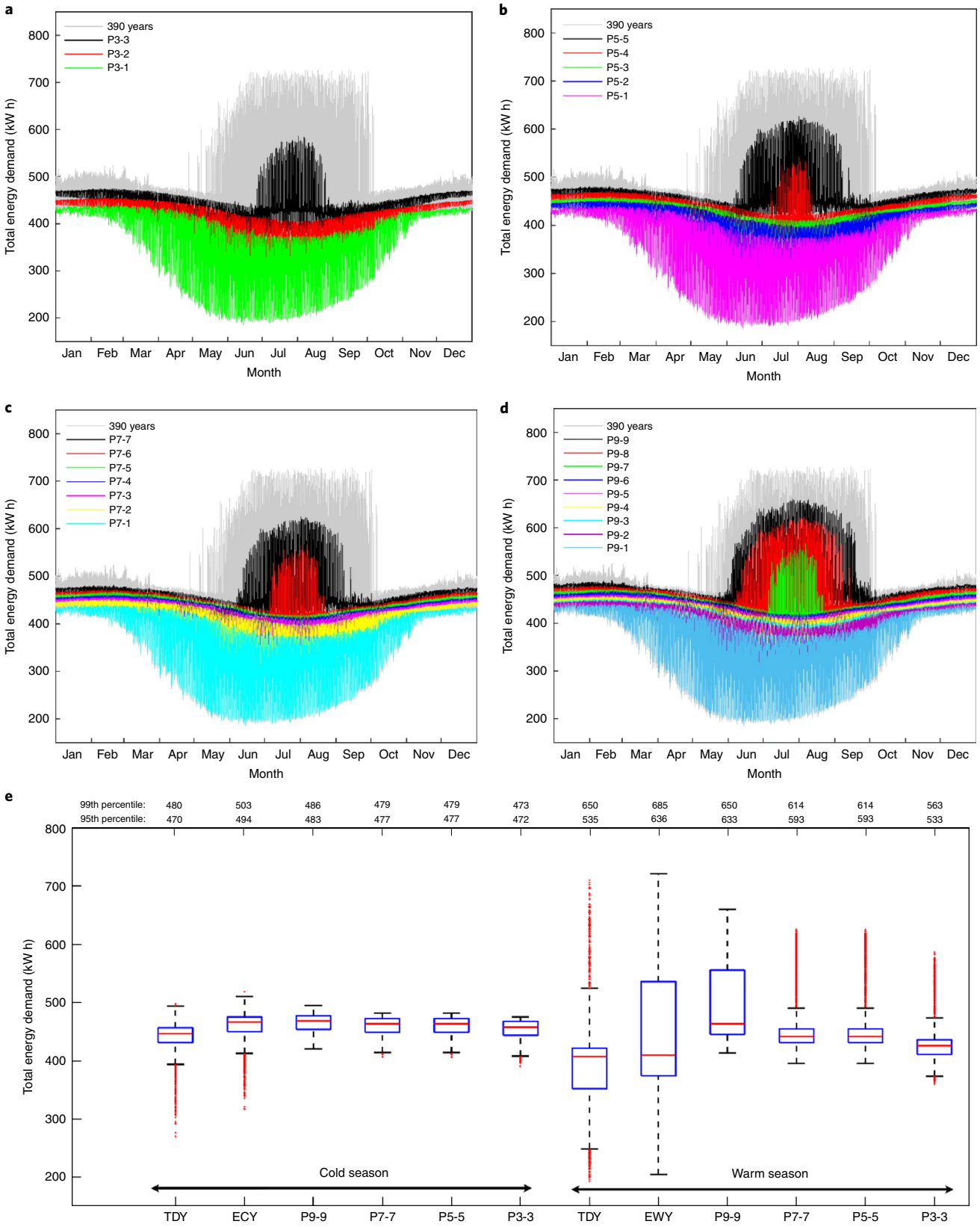


**Fig. 4 | Impacts of future climate variations on energy demand and renewable energy generation. a–d**, Hourly distribution of the total energy demand in Malmö during 2070–2099 for 13 climate scenarios (390 profiles, light-grey lines) and expected scenarios considering three (**a**), five (**b**), seven (**c**) and nine (**d**) sets of scenarios. **e**, Comparison of the distribution of hourly total energy demand of the representative urban area in Malmö during cold and warm seasons, considering typical (TDY), extreme cold (ECY) and extreme warm (EWY) years, as well as extreme high demand values of the expected scenarios with nine (P9-9), seven (P7-7), five (P5-5) and three (P3-3) sets of scenarios. The 95th and 99th percentiles of each case are written above the corresponding box plot.

the box plots, ECY and EWY cover a larger span of extreme conditions. The sets with a higher number of expected scenarios, such as P9, can be useful for estimating extremes; however, they do not cover the whole range of variations.

Therefore, to accurately estimate extreme conditions when using the expected scenarios, the number of scenarios should be increased. Such an extension is computationally expensive because it will exponentially increase the size of the scenario tree (when extending the number of scenarios for renewable energy potentials and grid conditions) during the energy system optimization. For example, considering nine climate scenarios can lead to a total of 531,441 scenarios when considering grid restrictions to a similar level. By considering both the expected and extreme scenarios and using two different optimization techniques, it is possible to handle the problem in a reasonable way while considering the influences of both extreme (LPHI) and non-extreme (HPLI) conditions.

### Climate-induced energy uncertainty and renewable integration

The approach introduced in this study (the hybrid stochastic-robust optimization (SRO) algorithm) considers both HPLI and LPHI conditions. The stochastic formulation considers the HPLI conditions, whereas the robust component guarantees smooth operation during extreme events (more details are presented in the Methods section). Three other methods were used to benchmark this approach, which represents uncertainty induced by climate on different levels (Table 1). Stochastic optimization (SO) considers HPLI scenarios through stochastic formulation without considering extreme events, robust optimization (RO) takes care of extreme events by using a robust technique without considering HPLI events and the deterministic (DT) model includes a deterministic scenario without considering HPLI and extreme events. Detailed descriptions of these different techniques are presented in Supplementary Note 7. The energy system was optimized to consider the net present value (that is, to represent the financial aspect of the project) and the grid integration level (level of energy autonomy) by using all the aforementioned methods. A Pareto front represents all the non-dominant solutions. When moving from one solution to another, the value of one objective function may improve at the sacrifice of the other. A comprehensive description of the formulation of the objective functions is presented in the Methods section.

To investigate the impact of both HPLI and extreme events, we selected four cities, namely Hudiksvall, Kalix, Linköping and Malmö, that represent four different climate zones in Sweden. Our investigation considered their renewable energy generation potential, which shows a significant variation when compared with the energy demand (a detailed illustration of the renewable energy generation of each city is presented in Supplementary Note 10). Of the four cities, Hudiksvall has the lowest renewable energy potential. The potential to integrate renewable energy technologies improves when moving from Hudiksvall to Kalix, Linköping and Malmö (Fig. 5e). Pareto fronts obtained for Hudiksvall using the SRO, SO and DT models showed similar objective function values (Fig. 5a). A clear separation of RO was observed, as could be observed for the other locations as well. The system designs obtained using SO show that the potential to integrate renewable energy technologies is up to 34.5% (16.5% above the SRO model in Fig. 5g) while reducing the net present value by 16.7% as a result of neglecting the extreme events (HD1 in Fig. 5a). However, these design solutions with higher renewable energy integration levels compared with SRO will lead to a power supply drop during an extreme event with a probability of up to 3% (30 times higher than the threshold value set (0.1%), see Fig. 5f). This clearly shows that maintaining power supply reliability during extreme events will retard renewable energy integration and add an additional cost to the system.

The renewable energy integration level increased up to 34% (based on SRO) in Kalix, where three Pareto fronts behaved similarly, as they did in Hudiksvall. However, we observed a clear separation of the objective function values obtained by the DT model when grid integration levels were low. The performance degradation brought about by CInU will lead to a notable performance gap for the design solutions obtained using the DT model (KL1 in Fig. 5b). A significant increase in the grid integration level was observed as a consequence of HPLI scenarios. For example, the grid integration level increased from 19.7 to 26.4% in certain instances, creating a performance gap of 34%. The performance gap will lead to the Pareto solutions being dominated by the design solutions obtained using both SO and SRO, as shown by PG in Fig. 5a–d, which presents the objective function values of DT design solutions after simulating them for the pool of scenarios considered for SO and SRO. Such a large performance gap will adversely affect the operation of the transmission network, making it difficult to accommodate distributed energy systems. In addition to the performance gap, we observed a break in power supply for the design obtained using SO and DT, similar to Hudiksvall.

In Linköping, renewable energy integration potential further increased, up to 56% (Fig. 5e). A clear separation of the Pareto fronts was observed for Linköping, in contrast to the results from both Hudiksvall and Kalix (Fig. 5c). We observed a notable improvement in net present value when moving from DT to the SO and SRO scenarios. In this specific instance, CInU is having a favourable impact because it reduces demand and improves renewable energy integration. Neglecting the CInU will lead to a pessimistic energy system design with higher net present values, potentially causing losses of up to €2.21 million while increasing the net present value by 19%, considering the lowest cost designs of the SRO and DT Pareto fronts (LN1 in Fig. 5c). Similarly, the loss of load probability increased up to 10% as a result of neglecting the extreme events when using SO (100 times higher than the threshold value set; see Fig. 5f). Therefore, one can conclude that considering CInU can bring favourable conditions to distributed energy systems. Although HPLI favours distributed energy systems, considering the HPLI scenarios through stochastic optimization will lead to a significant drop in the power supply reliability of up to 10%.

Of the four cities considered, Malmö is the most promising for renewable energy integration. The distributed energy system shows that the potential to integrate renewable energy technologies is higher than the annual energy demand of the system while contributing to the main transmission grid (Fig. 5f). The Pareto fronts

**Table 1 | Techniques used to represent climate uncertainty and extreme climate events**

| Name | Description | Method used to present climate | Optimization method |
|---|---|---|---|
| DT | Deterministic model with typical weather data | Typical downscaled year | Deterministic |
| RO | Data for extreme demand and renewable energy generation | Extreme climate scenarios | Robust |
| SO | Stochastic model using expected climate scenarios | Expected climate scenarios | Stochastic |
| SRO | Stochastic-robust model using expected and extreme climate scenarios | Expected and extreme climate scenarios | Stochastic-robust |

A comprehensive overview of the SRO and SRO-Ex algorithm is presented in the Methods section. A brief overview of the other approaches is presented in Supplementary 7.

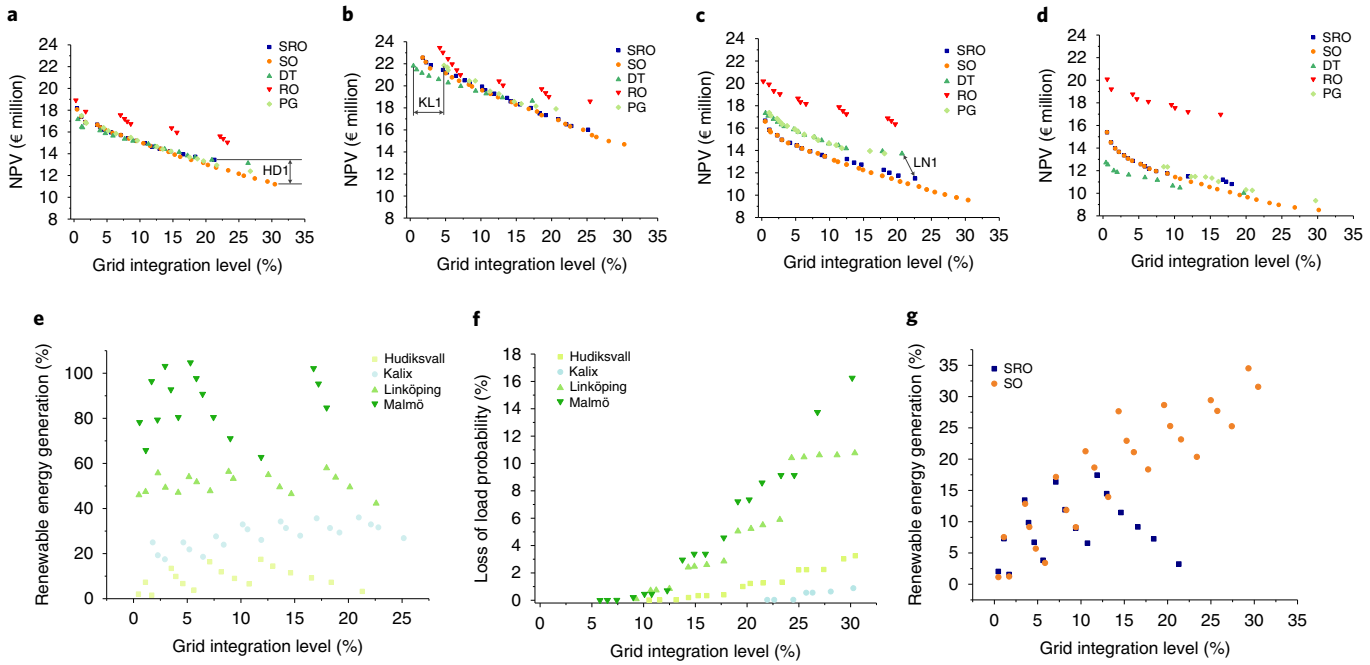


**Fig. 5 | Renewable energy generation potential in four cities. a–d**, The Pareto solutions obtained for the cities Hudiksvall (**a**), Kalix (**b**), Linköping (**c**) and Malmö (**d**). To understand the performance gap (PG), deterministic design solutions are simulated by using the pool of scenarios, and the objective function values obtained are presented as PG. **e**, The renewable energy integration levels for the Pareto solutions of the four cities. **f**, The loss of load probability as a consequence of neglecting extreme climate conditions. **g**, The renewable energy integration levels obtained, respectively, by the SRO and SO methods for Hudiksvall. HD1 in **a** and LN1 in **c** represent the deviation in the objective function values when using, respectively, the SO/SRO and DT/SRO techniques. KL1 in **b** represents the PG when using the DT model.

obtained by using different techniques show a notable split in objective function values when moving from one to another. The design solutions obtained by using the DT model presented the cheapest design solutions. However, HPLI scenarios will result in notable performance degradation (as marked by PG in Fig. 5d), which makes SRO and SO the dominant solutions. In this context, we observed performance degradation in both grid integration level and net present value. In addition, neglecting extreme events when using the SO model could result in a drop in power supply reliability (up to 16%).

Based on the results from the four representative cities, we conclude that the impacts of extreme climate events become more and more challenging when the penetration level of renewable energy technologies is increased. However, the Pareto fronts obtained by using RO show a very conservative picture of the energy system, having a very high net present value and low renewable penetration levels. Hence, considering extreme events by using a robust technique alone will no longer support the renewable energy integration process. These results demonstrate the importance of considering a hybrid approach that includes both stochastic and robust optimization techniques, like the one introduced in this study. This strategy will present a more optimistic picture of renewable energy integration while guaranteeing robust operation.

A clear separation of the obtained Pareto fronts is visible with improvements in renewable energy integration levels. This highlights the sensitivity of the method used to represent CInU. In addition, the loss of load probability and performance gap due to HPLI scenarios increased as a consequence of neglecting climate uncertainty and extreme events. This analysis clearly indicates that extreme events will notably reduce the renewable energy integration process by 16.5% in Hudiksvall. Retarding the integration of renewable energy technologies will lead to further dependence on fossil-fuel-based energy technologies, which will further accelerate climate change and increase climate-change-induced uncertainties, creating a vicious cycle. Hence, it is important to understand the potential to integrate renewable energy technologies that are resilient to climate change. Such potential was evaluated for 30 major cities in Sweden in this study.

## Renewable energy integration at the national scale

Sweden is divided into four climate zones, each of which follows its own building and energy regulations (see Fig. 6d). The 30 cities considered in this study represent the residential building stock in the country and more than 30% of Sweden's population. A clear difference in renewable energy integration potential is observed when moving from one climate zone to another. Except for Kalix and Sundsvall, respectively, in Climate Zones 1 and 2, the potential for renewable energy integration using solar photovoltaics and wind is less than 20% (Fig. 6a). The potential to integrate renewable energy technologies notably improves for Climate Zone 3 (Fig. 6b). Usually, direct grid integration of renewable energy technologies is possible where the renewable energy integration is below 25%. In Climate Zone 3, most of the cities (except Gnesta) have the potential to integrate renewable energy technologies that supply up to 30–50% of the annual energy demand. The level of renewable energy integration reaches above the annual demand in Malmö, Strömstad and Tjörn in Climate Zone 4 (Fig. 6c). Therefore, distributed energy systems represent a promising method for energy generation in Climate Zones 3 and 4, which accommodate renewable energy above 25% of the annual demand. More importantly, the potential to integrate renewable energy technologies such as solar photovoltaic and wind turbines in Climate Zones 3 and 4 are well above the present installed capacity. Hence, there is ample opportunity to harness these resources while guaranteeing robust operation of the energy infrastructure. Therefore, although climate-induced uncertainties and extreme events can challenge renewable energy integration, upgrading the methods used to design distributed energy systems

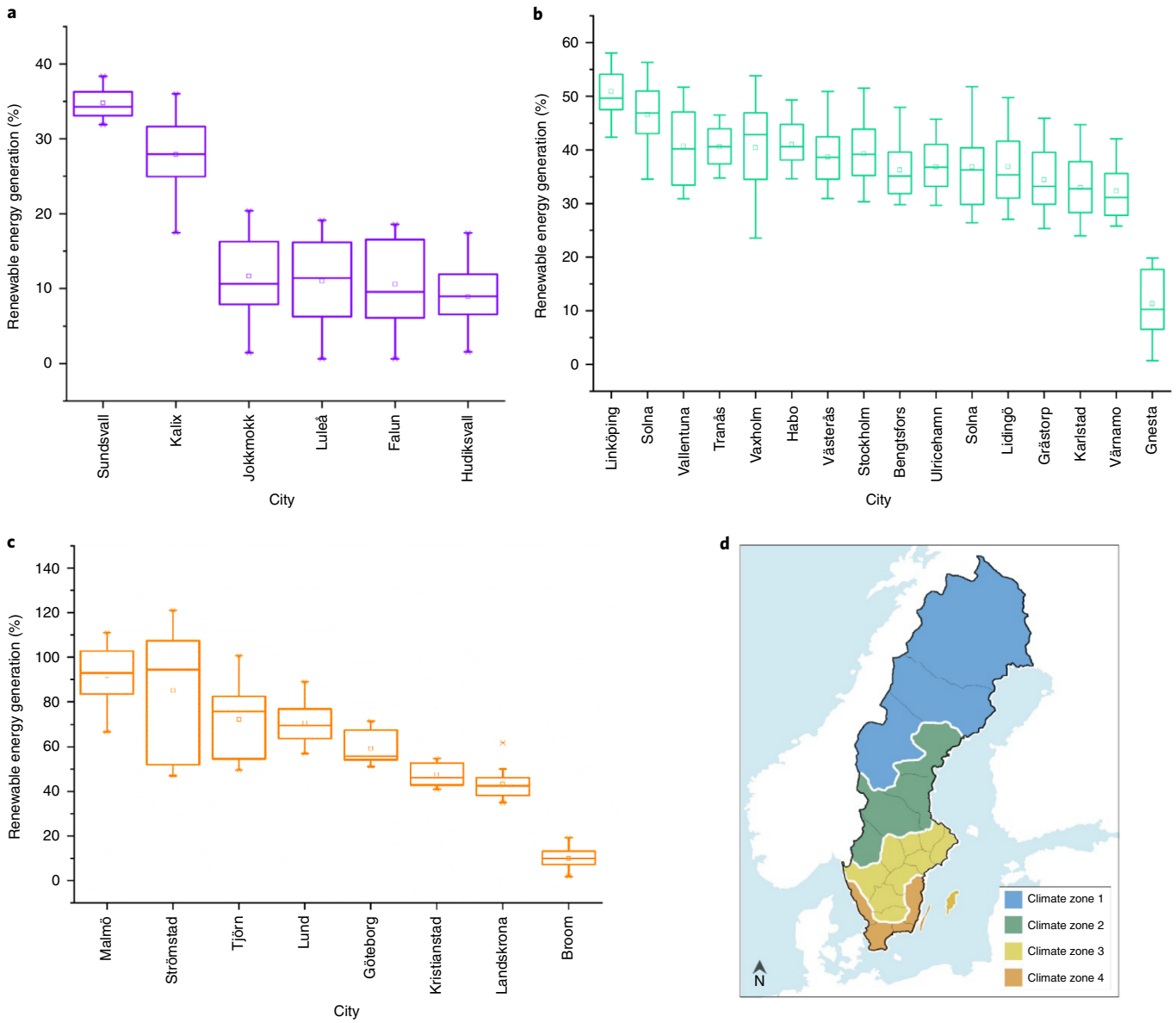


**Fig. 6 | Potential to integrate renewable energy technologies. a–c**, The climate resilience of the urban energy systems in 30 cities in Sweden is investigated in this study, and each city belongs to one of Sweden's four climate zones: Climate Zones 1 and 2 (**a**), Climate Zone 3 (**b**) and Climate Zone 4 (**c**). **d**, A map of Sweden showing the four climate zones.

can help to improve the renewable energy integration above 30% of the annual demand for a majority of the main cities in Sweden.

## Conclusions and future perspectives

Climate change induces variations that affect the urban energy system at different temporal scales, from changes in long-term patterns to short-term extreme conditions. Calculations based on typical weather conditions may reflect gradual changes; however, a robust design is highly dependent on considering extreme climatic conditions. In addition, it is important to consider HPLI conditions induced by climate change and quantify those when designing the energy system. To do so, in this study we introduced the concept of synthesizing expected scenarios and incorporating them into the energy system design process. Using a larger number of expected scenarios will help to introduce necessary deviations and extreme climate into the optimization process for energy system design. However, increasing the set of expected scenarios will increase the scenario tree and prolong the energy system optimization computation process. Therefore, it is important to split the process into two parts and present possible climate change variations and extreme events as separate time series. As a result, they can be analysed, respectively, by stochastic and robust optimization techniques during the energy system optimization. Multiple future climate scenarios should be used while synthesizing such time series, enabling analyses to consider CInU.

The case study for Sweden shows that renewable energy integration levels can be notably reduced when considering both HPLI and extreme events. In addition, HPLI events will create a performance gap of up to 20 and 34%, considering net present value and grid integration levels, respectively (considering 13 climate change scenarios). When integrating distributed energy systems into the transmission grid, such a significant increase in the grid integration level can cause many technical issues. Although stochastic models may represent long-term climate variations, these models do not guarantee robust operation of the energy system during extreme events. As a result, power supply reliability could drop by as much as 16% during

such events. Such a significant increase in the loss of load probability can easily lead to blackouts. Therefore, it is important to consider HPLI and extreme events when designing distributed energy systems. Quantifying the impacts of climate change and adapting the energy system designs appropriately will help to increase the renewable energy fraction up to 30% while guaranteeing robust operation.

## Methods

**Analytical approach.** Energy systems should possess the capability to manage climate variations without a significant drop in performance. Stochastic optimization, rather than robust optimization, is a better way to consider climate variations when formulating the objective functions[20], as presented in detail in Supplementary Note 5. Extreme climate occurs during short time spans (days to weeks) in comparison with the time span of the time series simulation (1 year). Scenarios corresponding to extreme climatic conditions will therefore have a lower probability when converted into a time series of 8,760 time steps. Consequently, it is difficult to consider them in the stochastic optimization process due to computational limitations (discussed in detail earlier). Therefore, it is important to consider climate variations and extreme climate events at two different levels by using a hybrid stochastic-robust optimization algorithm, which has previously been applied to unit commitment problems related to power systems[21,22] but has not yet been used for energy system design, as shown in Supplementary Note 5. However, it is difficult to translate climate relevant data into energy system relevant data and to create scenarios for stochastic-robust optimization.

**Representative weather data sets from climate models.** We synthesized hourly weather data considering 13 future climate scenarios for the 30-year span of 2070–2099 as the outputs of the Rossby Centre regional atmospheric model RCA4[23] (the fourth generation of the Rossby Centre RCM). We then used these data to create two groups of typical and extreme weather data sets (based on hourly and monthly distributions), as well as five expected scenarios.

RCMs are climate models that downscale global climate models (GCMs) dynamically to a regional scale. GCMs, forced by representative concentration pathways (RCPs), are used to simulate future climate conditions on a global scale, providing future climate scenarios. Because the spatial and temporal resolutions of GCM outputs are coarse, they need to be downscaled to finer resolutions by means of a statistical or dynamical downscaling technique[24]. Although the common practise for technical applications is statistical downscaling, it has the disadvantage of focusing on the long-term trends of climate change and underestimating extreme weather conditions. Compared with statistical downscaling, RCMs better represent topography and mesoscale processes, and have the advantage of generating physically consistent data sets across different variables with fine spatial and temporal resolutions. The weather data that are commonly used in energy simulations are mesoclimate data with hourly temporal resolution, and RCMs can provide such weather data for our simulations. For this work, RCA4 downscaled five GCMs, namely CNRM-CERFACS-CNRM-CM5, ICHEC-EC-EARTH, IPSL-IPSL-CM5A-MR, MOHC-HadGEM2-ES and MPI-M-MPI-ESM-LR (hereafter called CNRM, ICHEC, IPSL, HadGEM and MPI, respectively), to the spatial resolution of 12.5 km. These driving models were forced by three RCPs: CNRM and IPSL were forced by RCP4.5 and RCP8.5, and the rest by RCP2.6, RCP4.5 and RCP8.5. The combination of the models and scenarios used resulted in 13 future climate scenarios (these weather data sets are called 'RCM data' hereafter). Two types of synthesized weather data were created on the basis of the RCM data for optimizing energy system design: (1) typical and extreme weather scenarios (applied in reference and robust optimization algorithms) and (2) expected weather scenarios (applied in stochastic optimization).

**Typical and extreme weather scenarios.** We used the RCM data to synthesize two groups of representative weather data sets for a 30-year period. Each group includes three 1-year weather data sets: one for TDY, one for ECY and one for EWY[19]. The difference between the two groups lies in the time scale for choosing the representative data, that is, choosing the representative month or hour. Synthesizing TDY, ECY and EWY on a monthly basis is explained in detail in ref. [19]. In short, the method is based on Finkelstein–Schafer statistics: choosing the single month with the closest cumulative distribution temperature to whole months ($13 \times 30 = 390$ months in this case). This will provide a TDY, whereas for ECY and EWY, the months with the largest differences are chosen.

The method was developed further to track all the possible extremes at each time step for any climate variable. To do so, the typical and extreme values of a climate variable were chosen according to the distribution of the variable at each time step (hour), considering all the years and climate scenarios ($13 \times 30 = 390$ data points at each hour). This results in three time series (with the length of 8,760 h), each containing the most typical, the lowest and the highest values at each hour. Note that the data generated are not supposed to reflect realistic weather sequences because they do not reflect realistic variations of the climate system (unlike the monthly based TDY, ECY and EWY, which reflect realistic variations). However, each hourly value is a possible future condition (according to climate models) that can challenge the energy system. In Fig. 3, all 390 possible future conditions (light-grey lines) are compared with the monthly and hourly based typical and extreme data sets.

**Expected weather scenarios.** We synthesized a number of scenarios to represent future weather conditions, each containing a time series of 8,760 time steps. Like the previous approach, all 390 years of weather data were accommodated in 1 year. By generating the cumulative distribution of values at each hour and calculating their percentiles, the values (for example, wind speed) for different probabilities could be calculated. For example, if wind speed varied between 0 and 20 m s$^{-1}$ during 1 year, by dividing the range of values into nine time series (nine expected scenarios), the first 5% (percentile of 0–5%) represented the lowest wind speed values during the whole year, whereas the last 5% (percentile of 95–100%) represented the highest. In other words, the first 5% is a pseudo-sequential time series with one value at each time step that represents the percentiles between 0 and 5%, whereas the last 5% represents percentiles between 95 and 100%. We generated four groups of expected scenarios in this work by synthesizing pseudo-sequential time series considering three (20-60-20%), five (10-20-40-20-10%), seven (10-15-15-20-15-15-10%) and nine (5-5-15-15-20-15-15-5-5%) sequences, called 'expected scenarios' hereafter. Note that the time series of the expected scenarios do not represent realistic variations of the climate system. Therefore, two alternative representations considering the fluctuations in demand and renewable energy generation are presented in Supplementary Note 6, and those clearly represent the influence of uncertainties on the Pareto fronts. The described method can be applied to any variable, with many possible values at each time step, to create the expected scenarios for renewable generation potentials and energy demand. A more descriptive explanation of the method is presented in Supplementary Note 4.

**Computational model for energy system optimization.** We developed a computational algorithm in this study to accommodate climate resilience in the energy system design process by extending the entire time series approach explained in Supplementary Note 5. We used robust programming to compute the performance related to the reliability of the system (by introducing constraints to guarantee a minimum performance level) and used stochastic programming to evaluate objective function values considering climate variations. The two approaches have been hybridized for unit commitment problems related to power systems[21,22], although it has not been applied to energy system design before. We used the dispatch strategy proposed by Perera et al.[5] (as explained in Supplementary Note 3) to consider complex interactions for the unit commitment problem, addressing the limitations in present state of the art models. We used graphical processor unit (GPU) computing to increase the number of scenarios through large-scale parallelization while reducing the computational time.

**Outline of the energy system.** The energy hub we considered in this study (a description of the design of the energy hub is presented in Supplementary Note 1) is operated in connection with the local electricity grid. It injects electricity into the grid when there is excess generation (and also when the cost of selling is competitive) and purchases electricity from the grid to cater for the mismatch between demand and generation. We introduced grid curtailments both for selling electricity to the grid and for purchasing electricity from it to guarantee grid stability. The energy hub consists of wind turbines and photovoltaic panels, which are non-dispatchable energy technologies. We used an internal combustion engine as the dispatchable source. A battery bank was used as the energy storage, to help the internal combustion engine and grid absorb fluctuations in both demand and generation. We performed building simulations for the residential building stock of 30 cities in Sweden using a verified model, which is thoroughly discussed in a previous report[6]. We used the energy demand of a combination of a certain number of buildings to represent a typical urban area in each city. We assumed that the heating demand was provided using heat pumps.

**Decision space variables.** For the decision space variables, we considered variables related to both system design and operation strategy. Time series simulation was used to map decision space variables into the objective space, as explained before. The decision space includes both discrete and continuous variables. We represented variables related to system design using discrete variables, while continuous variables were used to represent the dispatch strategy. The number of wind turbines, photovoltaic panels and battery banks, as well as the size of the internal combustion generator, were considered as decision space variables. The technology used for photovoltaic panels and the performance curve of wind turbines notably influence the power generation and cost. Hence, the type of wind turbine and photovoltaic panel were also considered as decision space variables, along with their capacity.

**Formulation of objective functions and constraints.** The computational model formulates the objective functions, and constraints map decision space variables into the objective space. Energy system optimization is performed using a simulation-based optimization algorithm. As shown in Fig. 2, the decision space variables are mapped into the objective space through a life cycle simulation that computes the objective function values and constraint violation (in case there is one). Collecting techno-economic data helps to formulate the model used for

the simulation. RCMs and building simulations help to develop the scenarios needed for stochastic and robust conditions. Scenarios related to stochastic and robust elements use a similar computational model for time series simulation. Hence, the computational model corresponding to this part is common for both. It is introduced as the Simulation block in Fig. 2. Objective function values are computed using the Stochastic block, which corresponds to stochastic optimization. Constraint violation is evaluated using the Robust block.

**Simulation block.** The Simulation block is the computational model common to both robust and stochastic elements. Evaluation of the energy flow based on hourly simulation is the part common to both sections. Hourly wind speed, solar irradiation, energy demand and other factors are taken as the input to the Simulation block, which determines the renewable power generation within the system. Based on the power generation, interactions with the grid, energy storage and the internal combustion generator are determined using the dispatch strategy. A detailed description of the energy flow model is presented in Supplementary Note 2.

**Robust block formulating constraints.** Performance indicators that guarantee robust operation under extreme scenarios are computed through the Robust block. The reliability of the system is assumed to be the main priority, that is, maintaining a reliable power supply during normal conditions as well as extreme climate events. Hence, loss of load probability is considered as a constraint in the optimization problem. Loss of load probability has been widely used in the literature as a measure to evaluate the reliability of power systems[25,26]. Energy systems are simulated considering extreme scenarios, and energy flow is computed using the Simulation block to compute loss of load probability. Loss of power supply (LPS), computed using equation (1), will occur whenever there exists a mismatch between renewable power generation and demand that cannot be provided using the battery bank, internal combustion generator and grid.

$$\mathrm{LPS}_{t,s} = \mathrm{ELD}_{t,s} - P^{\mathrm{RE}}_{t,s} - P^{\mathrm{ICG}}_{\mathrm{Max}} - P^{\mathrm{Bat-Max}}_{t,s} - \mathrm{IG}_{\mathrm{Lim}},\ \forall t \in T,\ \forall s \in \pi \tag{1}$$

In equation (1), $P^{\mathrm{Bat-Max}}_{t,s}$, $\mathrm{IG}_{\mathrm{Lim}}$, $P^{\mathrm{ICG}}_{\mathrm{Max}}$ and $\mathrm{ELD}_{t,s}$ denote maximum possible power flow from the battery bank (depending on the state of charge), maximum power purchased from the grid, nominal power of the internal combustion generator and electricity load demand, respectively. $P^{\mathrm{RE}}_{t,s}$ denotes renewable energy generation using both photovoltaic panels and wind turbines. $t$ denotes a time step of one hour and belongs to the set of $T$, which describe the entire time series, while $s$ denotes a scenario that belongs to the set of $\pi$.

The loss of load probability (LOLP) is computed using equation (2).

$$\mathrm{LOLP} = \mathrm{Max}_{s\in\pi}\left(\frac{\sum_{\forall t\in T}\mathrm{LPS}_{t,s}}{\sum_{\forall t\in T}\mathrm{ELD}_{t,s}}, 0\right) \tag{2}$$

The main weakness of equation (2) is that it considers the entire time series (a period of 1 year) when computing the loss of load probability. This might lead to erroneous results (as it averages the condition over 1 year) when considering extreme events that last for a short period, leading to higher loss of load probability during extreme climate events. To avoid this issue LOLP-Ex is introduced as an improved replacement, given by equation (3).

$$\mathrm{LOLP-Ex} = \mathrm{Max}_{s\in\pi}\left(\mathrm{Max}_{t\in T}\frac{\sum_{t=t_0}^{t=t+d}\mathrm{LPS}_{t,s}}{\sum_{t=t}^{t=t+d}\mathrm{ELD}_{t,s}}, 0\right) \tag{3}$$

In Equation (3), $d$ denotes the time period the extreme climate condition is expected to last.

**Stochastic block formulating objective functions.** Stochastic-robust optimization has recently become popular for dispatch optimization problems[27]. Different methods have been used in these studies to consider both stochastic and robust aspects of energy system operation. In most instances, stochastic and robust parts of the objective function are combined by weighting the impact of each[27]. In certain instances, a penalty cost is introduced through robust programming[28], which is quite similar to introducing it as a constraint. When moving from dispatch optimization to energy system design, the context of the problem changes notably. Due to shorter time spans (mainly) during extreme climate conditions and the relatively low frequency of occurrence, the weight that should be assigned to the robust part of the objective function will be quite low. Hence, it is only considered as a constraint in the formulation of the optimization problem. Net present values of the system and grid integration level are considered as the objective functions. The computational model introduced in the common block is used to simulate energy flow within the system. Based on the energy flow, the cash flow of the system is computed for different scenarios within the Stochastic block. Similarly, the autonomy level of the system is computed based on the hourly simulation.

**Net present value.** The expected net present value ($E$(NPV)) is computed considering all the cash flows that have taken place within the system's lifetime. The net present value includes two main parts: initial capital cost and operation and maintenance cost. The price uncertainty related to the initial capital cost, which includes acquisition and installation costs, was not considered in this study. Hence, the initial capital cost was computed only considering the deterministic part. Introducing scenarios that consider climate and grid uncertainty will result in a notable change in the operation and maintenance cost. The operation and maintenance cost consists of two main components: fixed costs ($\mathrm{OM}^{\mathrm{Fixed}}$) and variable costs ($\mathrm{OM}^{\mathrm{Variable}}$). $\mathrm{OM}^{\mathrm{Fixed}}$ considers recurrent annual cash flows (such as the maintenance costs of wind turbines, photovoltaic panels and fuel, and the operation costs of an internal combustion engine). $\mathrm{OM}^{\mathrm{Variable}}$ considers the replacement cost of internal combustion engines and battery banks. The replacement time for the internal combustion engine is determined by considering the operating hours and rain-flow algorithm using the common block. Finally, the net present value (NPV) is calculated using equation (4).

$$E(\mathrm{NPV}) = \mathrm{ICC} + \sum_{\forall s\in\Omega}\delta_s\Big[\sum_{\forall c\in C}(\mathrm{OM}^{\mathrm{Fixed}}_{c,s}\mathrm{CRF}_c) + \sum_{\forall h\in H}\sum_{\forall c\in C}\mathrm{PRI}^{l}\mathrm{OM}^{\mathrm{Variable}}_{c,h,s}\Big], \quad \forall t\in T,\ \forall s\in\Psi, \forall c\in C, \forall h\in H \tag{4}$$

In equation (4), $\mathrm{CRF}_c$ and ICC denote the capital recovery factor for the $c$th component and initial capital cost, respectively. PRI denotes the real interest rate calculated using both the interest rates for investment and the local market annual inflation ratio. $\delta$ and $h$ denote the expected value of the scenario and the year considered.

**Grid integration level.** The autonomy level of a distributed energy system depends on the level of its interactions with the grid. Maintaining minimum grid interactions is always recommended from the perspective of grid stability. Therefore, grid curtailments are considered for both selling and purchasing electricity to and from the grid. According to Perera et al.[5], the autonomy level of a distributed energy system can be measured in different ways. In this study, grid integration (GI) was evaluated on the basis of the units purchased form the grid (equation (5)) to maintain a stable operation of the distributed energy system.

$$E(\mathrm{GI})_{\forall s\in\Psi} = \sum_{\forall s\in\Omega}\delta_s\frac{\sum_{\forall t\in T}P^{\mathrm{FG}}_{t,s}}{\sum_{\forall t\in T}\mathrm{ELD}_{t,s}}, \forall t\in T, \forall s\in\Psi \tag{5}$$

In equation (5), $P^{\mathrm{FG}}_{t,s}$ denotes the energy purchased from the grid.

**Implementation of the computational algorithm.** Simulation-based optimization is a time-consuming activity, and it becomes more challenging when accommodating a large number of scenarios that demand lengthy simulations. Hence, efficient implementation of the computational program plays a vital role. To accomplish this objective, we introduced GPU computing into this study to conduct time series simulations (the details are described in Supplementary Notes 8 and 9). GPU computing facilitates large-scale parallelization of a computational program. As a result, GPU computing has already been used in different fields, such as image processing, machine learning, bioinformatics and others. However, GPU computing is not well known among the energy system design community, despite its potential to speed up computational processes. When considering stochastic optimization, GPU computing makes it feasible to handle a large number of scenarios within a reasonable computational time. For example, the number of scenarios considered in this work (5,835 scenarios) is much higher than the number of scenarios considered by Narayan and Ponnambalam (200 scenarios)[29].

Previously, for ease of understanding, the objective functions were formulated using three blocks. The computational algorithm begins in a similar manner, following the mathematical model. The techno-economic and weather data are collected and input to the computational algorithm. The Simulation block (considered as one part), which includes the set of computational models, is divided into a stochastic and a robust part, and implemented in both the central processing unit (CPU) and the GPU. The scenarios related to the stochastic part are implemented in the GPU, which supports large-scale parallelization. The scenarios related to the robust and deterministic parts are implemented in the CPU. Subsequently, the objective function values and constraints are computed in the CPU, aggregating the computations performed in both the CPU and GPU. Based on the objective function values, the population and archive are updated following the dominance check using the CPU.

**Optimization algorithm.** Different techniques based on convex optimization, non-convex optimization, linear programming, mixed integer linear programming and heuristic methods have been used to design distributed energy systems. Heuristic methods have been shown to be an effective way to design distributed energy systems in recent years[30]. Soroudi and Amraee[31] highlighted the importance of developing algorithms based on heuristic methods to design energy systems under uncertainty. Heuristic algorithms have been widely used for both stochastic[32] and robust[33] optimization problems. This study used the steady-state ε-dominance method to conduct Pareto optimization. We used the constraint tournament method to handle the constraints in the optimization process. A polynomial

mutation operator and a simulated binary crossover operator were used, along with differential evolutionary operators in the reproduction of the population. An extended explanation of the operators used for the optimization can be found in ref. [34]. The net present value and grid integration level, introduced before, were used as the objective functions.

A comprehensive description of the energy flow model, dispatch strategy and optimization algorithms used to benchmark the method are presented in Supplementary Notes 2 and 3.

## Data availability

The data relevant to the energy and climate models not found in the in Supplementary Notes 1–3 are available from the corresponding author upon reasonable request. The raw climate data are available through Coordinated Regional Climate Downscaling Experiment (http://www.cordex.org/). Source data for Figs. 3–6 are provided with the paper.

## Code availability

The computational code is available from the corresponding author for academic purposes upon reasonable request.

Received: 14 September 2018; Accepted: 14 January 2020;
Published online: 17 February 2020

## References

1. IPCC *Climate Change 2014: Synthesis Report* (eds Core Writing Team, Pachauri, R. K. & Meyer L. A.) (IPCC, 2014).
2. IPCC *Managing the Risks of Extreme Events and Disasters to Advance Climate Change Adaptation: Special Report of the Intergovernmental Panel on Climate Change* (Cambridge Univ. Press, 2012); https://doi.org/10.1017/CBO9781139177245.
3. *The Global Risks Report 2016* (World Economic Forum, 2016); https://www.weforum.org/reports/the-global-risks-report-2016/.
4. *World Urbanization Prospects: The 2018 Revision* (United Nations, Department of Economic and Social Affairs, 2019).
5. Perera, A. T. D., Nik, V. M., Mauree, D. & Scartezzini, J.-L. Electrical hubs: an effective way to integrate non-dispatchable renewable energy sources with minimum impact to the grid. *Appl. Energy* **190**, 232–248 (2017).
6. Nik, V. M. & Sasic Kalagasidis, A. Impact study of the climate change on the energy performance of the building stock in Stockholm considering four climate uncertainties. *Build. Environ.* **60**, 291–304 (2013).
7. Stern, P. C., Sovacool, B. K. & Dietz, T. Towards a science of climate and energy choices. *Nat. Clim. Change* **6**, 547–555 (2016).
8. Pryor, S. C., Schoof, J. T. & Barthelmie, R. J. Winds of change?: Projections of near-surface winds under climate change scenarios. *Geophys. Res. Lett.* **33**, L11702 (2006).
9. Sailor, D. J., Smith, M. & Hart, M. Climate change implications for wind power resources in the Northwest United States. *Renew. Energy* **33**, 2393–2406 (2008).
10. Wang, B., Ke, R.-Y., Yuan, X.-C. & Wei, Y.-M. China's regional assessment of renewable energy vulnerability to climate change. *Renew. Sustain. Energy Rev.* **40**, 185–195 (2014).
11. Auffhammer, M., Baylis, P. & Hausman, C. H. Climate change is projected to have severe impacts on the frequency and intensity of peak electricity demand across the United States. *Proc. Natl Acad. Sci. USA* **114**, 1886–1891 (2017).
12. Sharifi, A. & Yamagata, Y. Principles and criteria for assessing urban energy resilience: a literature review. *Renew. Sustain. Energy Rev.* **60**, 1654–1677 (2016).
13. Nik, V. *Hygrothermal Simulations of Buildings Concerning Uncertainties of the Future Climate*. PhD thesis, Chalmers Univ. of Technology (2012).
14. Panteli, M. & Mancarella, P. Influence of extreme weather and climate change on the resilience of power systems: impacts and possible mitigation strategies. *Electr. Power Syst. Res.* **127**, 259–270 (2015).
15. Dowling, P. The impact of climate change on the European energy system. *Energy Policy* **60**, 406–417 (2013).
16. IPCC *Climate Change 2013: The Physical Science Basis* (eds Stocker, T. F. et al.) (Cambridge Univ. Press, 2013).
17. Herrera, M. et al. A review of current and future weather data for building simulation. Build. Serv. Eng. Res. Technol. 38, 602–627 (2017).
18. Hall, I. J., Prairie, R. R., Anderson, H. E. & Boes, E. C. Generation of a typical meteorological year. In Proc. Conference: Analysis for solar heating and cooling (Office of Scientific and Technical Information, 1978); http://www.osti.gov/scitech/biblio/7013202
19. Nik, V. M. Making energy simulation easier for future climate – synthesizing typical and extreme weather data sets out of regional climate models (RCMs). *Appl. Energy* **177**, 204–226 (2016).
20. Mavromatidis, G., Orehounig, K. & Carmeliet, J. Comparison of alternative decision-making criteria in a two-stage stochastic program for the design of distributed energy systems under uncertainty. *Energy* **156**, 709–724 (2018).
21. Zhao, C. & Guan, Y. Unified stochastic and robust unit commitment. *IEEE Trans. Power Syst.* **28**, 3353–3361 (2013).
22. Baringo, A. & Baringo, L. A stochastic adaptive robust optimization approach for the offering strategy of a virtual power plant. *IEEE Trans. Power Syst.* **32**, 3492–3504 (2017).
23. Samuelsson, P. et al. *The Surface Processes of the Rossby Centreregional Atmospheric Climate Model (RCA4)* (Swedish Meteorological and Hydrological Institute, 2015); https://www.smhi.se/en/publications/the-surfaceprocesses-of-the-rossby-centreregional-atmospheric-climate-modelrca4-1.89801.
24. Hellström, C., Chen, D., Achberger, C. & Räisänen, J. Comparison of climate change scenarios for Sweden based on statistical and dynamical downscaling of monthly precipitation. *Clim. Res.* **19**, 45–55 (2001).
25. Perera, A. T. D., Nik, V. M., Mauree, D. & Scartezzini, J.-L. An integrated approach to design site specific distributed electrical hubs combining optimization, multi-criterion assessment and decision making. *Energy* **134**, 103–120 (2017).
26. Celik, A. N. Effect of different load profiles on the loss-of-load probability of stand-alone photovoltaic systems. *Renew. Energy* **32**, 2096–2115 (2007).
27. Ji, L., Niu, D. X. & Huang, G. H. An inexact two-stage stochastic robust programming for residential micro-grid management-based on random demand. *Energy* **67**, 186–199 (2014).
28. Bagheri, A., Zhao, C. & Guo, Y. Data-driven chance-constrained stochastic unit commitment under wind power uncertainty. In *2017 IEEE Power & Energy Society General Meeting* 1–5 (IEEE, 2017); https://doi.org/10.1109/PESGM.2017.8273948.
29. Narayan, A. & Ponnambalam, K. Risk-averse stochastic programming approach for microgrid planning under uncertainty. *Renew. Energy* **101**, 399–408 (2017).
30. Agustín, J. L. B. & López, R. D. Efficient design of hybrid renewable energy systems using evolutionary algorithms. *Energy Convers. Manag.* **50**, 479–489 (2010).
31. Soroudi, A. & Amraee, T. Decision making under uncertainty in energy systems: state of the art. *Renew. Sustain. Energy Rev.* **28**, 376–384 (2013).
32. Fouskakis, D. & Draper, D. Stochastic optimization: a review. *Int. Stat. Rev.* **70**, 315–349 (2002).
33. Beyer, H.-G. & Sendhoff, B. Robust optimization – a comprehensive survey. *Comput. Methods Appl. Mech. Eng.* **196**, 3190–3218 (2007).
34. Perera, A. T. D., Attalage, R. A., Perera, K. K. C. K. & Dassanayake, V. P. C. Converting existing internal combustion generator (ICG) systems into HESs in standalone applications. Energy Convers. Manag. 74, 237–248 (2013).

## Acknowledgements

We thank E. Kjellström, G. Strandberg and G. Nikulin from the Rossby Centre at the Swedish Meteorological and Hydrological Institute (SMHI) for their help with the climate data and assessment. We thank E. Davin of ETH Zurich for his interesting insights in relation to this study. We also thank K. Javanroodi for creating the map of Sweden for this publication. This work was supported by the Swiss Competence Center for Energy Research SCCER FEEB&D of the Swiss Innovation Agency Innosuisse (CTI.2014.0119), the Swedish Research Council for Sustainable Development (Formas 2016-20123), the Assistant Secretary for Energy Efficiency and Renewable Energy, Office of Building Technologies of the United States Department of Energy (Contract no. DE-AC02-05CH11231) and the Swedish national strategic research program BECC and 398 MERGE. Some of the computations were performed on resources provided by the Swedish National Infrastructure for Computing (SNIC) at the National Supercomputer Centre in Sweden (NSC).

## Author contributions

A.T.D.P., V.M.N., D.C., J.L.S. and T.H. designed the research. V.M.N. synthesized the climate data and conducted the uncertainty analysis and impact assessment of climate change on energy demand and renewable generation. A.T.D.P. developed the energy system optimization algorithm and conducted the energy system analysis. A.T.D.P., V.M.N., D.C., J.L.S. and T.H. wrote the manuscript.

## Competing interests

The authors declare no competing interests.

## Additional information

**Supplementary information** is available for this paper at https://doi.org/10.1038/s41560-020-0558-0.

**Correspondence and requests for materials** should be addressed to A.T.D.P.

**Reprints and permissions information** is available at www.nature.com/reprints.

**Publisher's note** Springer Nature remains neutral with regard to jurisdictional claims in published maps and institutional affiliations.